Master Thesis

Quantum Criticality in the Transverse Field Random Ising Model

Kristoffer Aronsen

Condensed Matter Theory, Department of Physics,
School of Engineering Sciences
Royal Institute of Technology, SE-106 91 Stockholm, Sweden

Stockholm, Sweden 2019

Typeset in LaTeX

Abstract

In this thesis the critical behaviour at the quantum phase transition of a transverse field random Ising chain is studied by mapping it to corresponding two-dimensional classical model. Monte Carlo simulations using the Wolff algorithm are performed in order to sample the system configurations. The critical point of the transition is located by measuring the Binder cumulant. An analysis of finite size scaling corrections is performed and it is demonstrated that a higher order correction to scaling is visible. The dynamic scaling of the system is studied, and it is shown that by taking proper account of scaling corrections the analytic prediction of activated dynamic scaling is observed. Average and typical correlations are measured for the system at the critical point and the scaling behaviour obtained is compared to analytical results. A discrepancy between the numerical and analytical value for the critical exponent of the average correlation is found. The scaling behaviour of the typical correlation is found to align well with the analytic value.

Key words: Transverse field random Ising chain, Monte Carlo simulation, Wolff algorithm, critical exponents, finite size scaling, quantum phase transition.

Preface

This thesis is the result of 12 months work between June 2018 and June 2019, for the degree of Master of Science in Engineering, in the Physics Department of KTH Royal Institute of Technology, Sweden. The work has been carried out at the Condensed Matter group and has been supervised by Prof. Mats Wallin.

Acknowledgements

Contents

Chapter 1

Introduction

The study of phase transitions is of particular interest in physics due to what is known today as the universality hypothesis, the observation that systems vastly different in the microscopic perspective shows asymptotically identical behaviour near a phase transition[1].

The most studied model within the area of statistical physics is probably the Ising model. Its main virtue is its simplicity and it has been an important source of understanding for the concepts of phase transitions and universality. It was for this model that Kadanoff presented his idea of block spins[2]. Kadanoff's work in turn lead Wilson to develop the method of the renormalization group, which has provided insight into both the nature of the critical exponents of phase transitions, and an explanation for the origin of universality through the fixed points of the renormalization group flow[3].

In the realm of quantum physics there is a model aptly known as the quantum Ising model, due to its similar shape to the classical model. It was shown by Suzuki[4] that the statistics of the quantum Ising model can be studied in terms of the classical Ising model through a mapping, which will be introduced in full detail in Sec. 2.4. One particular property of the mapping is that it takes a d-dimensional quantum system to a $(d+1)$-dimensional classical system.

Within the quantum framework a new type of phase transition appears, distinguished from the phase transitions of classical physics in that it occurs at zero temperature. Classically zero temperature implies that no fluctuations are possible, which prohibits phase transitions from taking place. A quantum system however is subject to quantum fluctuations even at absolute zero temperature, and as such phase transitions can occur. The quantum Ising model exhibits such a transition when exposed to a magnetic field transverse to the Ising spin axis. At zero magnetic field the spins are all aligned in the same direction, but as the field is tuned up quantum tunneling allows the individual spins to fluctuate between parallel and antiparallel. At some point the system becomes completely paramagnetic[5].

Quantum Ising magnets in a transverse field can be studied experimentally and at low temperatures signs of the theoretically predicted zero temperature phase transition is observable. This has for instance been done by Bitko, Rosenbaum and Aeppli[6] for Ho atoms in $LiHoF_4$ crystals, and more recently by Coldea et al.[7] for Co atoms in $CoNb_2O_6$.

In 1992 D. Fisher presented results for a generalization of the transverse field Ising model where both the field and the exchange couplings between spins are random variables from two arbitrary distributions[8, 9]. Each pair of spins are coupled with each other by a random coupling, and each site experiences a random field. The analysis was performed for the one-dimensional model, which by the aforementioned mapping corresponds to a two-dimensional classical system. This system exhibits a quantum phase transition as the average of the random field variables is increased beyond a critical value. Fisher showed that the critical behaviour of the system near the phase transition is rather unusual. In particular the average correlation and the typical correlation diverge with differing critical exponents, and the system undergoes what is known as activated dynamic scaling[5].

In a study by Pich and Young[10, 11] an incarnation of the random transverse field Ising model was simulated numerically to test the predictions by Fisher. However, the data they presented shows substantial uncertainty and the scaling results were not completely convincing.

In this thesis the same numerical analysis has been performed as in the study by Pich and Young with the aim to reduce the uncertainty and investigate whether this produces better estimates for the critical exponents due to Fisher. It is found that some of the scaling results can be considerably improved by considering corrections to scaling, which is the main result of this thesis. In Ch. 2 a review of some theoretical concepts relevant to the work in this thesis is presented. Chapter 3 details the theory regarding the numerical methods used and the implementation. In Ch. 4 the results of the numerical study is presented, and in Ch. 5 a summary and discussion, followed by an outlook are given.

Chapter 2

Theoretical Background

In this chapter various theoretical aspects are introduced. First a brief overview of statistical mechanics is given. The theory of critical phenomena, critical exponents and finite size scaling is reviewed. Thereafter the random transverse field Ising model is introduced. The mapping of the quantum Ising model to a corresponding classical model is derived in detail, and specifics of the mapping are discussed. Lastly the analytical results due to Fisher for the random transverse field Ising model are presented.

2.1 Equilibrium Statistical Mechanics

The problem when attempting to study physical systems on a microscopic level is that the sheer number of particles in a real world system is so large that treating each of them using classical equations of motion becomes impossible. Statistical mechanics is an area of physics which attempts to sidestep this problem by treating systems with probabilistic methods rather than by directly studying the dynamics of each particle. The central idea in statistical mechanics is that a system has a probability of being in any one particular of its microscopic states ω. Each state ω is defined by a specific configuration of the systems' degrees of freedom. In the study of equilibrium systems it can be shown that the probability of a state ω is given by the Boltzmann distribution

$$P\left(\omega\right) = \frac{1}{Z}e^{-\beta H(\omega)}, \tag{2.1}$$

where $\beta = \frac{1}{k_B T}$ is the inverse temperature and $H\left(\omega\right)$ is the Hamiltonian or energy of the system in state ω. The prefactor Z is called the partition function of the

system, and acts as a normalizing constant. For a discrete set of states it is defined as

$$Z = \sum_{\omega \in \Omega} e^{-\beta H(\omega)}, \tag{2.2}$$

where Ω denotes state space of the system. The partition function is a rather important function as it turns out, since it is possible to extract essentially all macroscopic information about the system from it. Macroscopic properties of the system are given as expectation values. Given a quantity $A(\omega)$ which is a function of the configuration of the system the expectation of A is given as

$$\langle A \rangle = \sum_{\omega \in \Omega} A(\omega) P(\omega)$$
$$= \frac{1}{Z} \sum_{\omega \in \Omega} A(\omega) e^{-\beta H(\omega)}. \tag{2.3}$$

Many such expectations can be computed directly from the partition function. For instance the expectation of the energy of the system is related to the derivative of Z with regards to β.

$$\frac{\partial Z}{\partial \beta} = -\sum_{\omega \in \Omega} H(\omega) e^{-\beta H(\omega)}$$
$$= -Z \langle H \rangle, \tag{2.4}$$

and so the expectation of the energy is

$$\langle H \rangle = -\frac{1}{Z} \frac{\partial Z}{\partial \beta} = -\frac{\partial \log Z}{\partial \beta}. \tag{2.5}$$

It is therefore desirable to be able to determine the partition function, but unfortunately this happens to be rather difficult for most systems. More often expectations are measured directly using numerical methods such as Monte Carlo simulations instead.

2.2   Critical Phenomena

The subject of critical phenomena is the study of systems near a phase transition. This has interested physicists due to its difficulty. Another reason for studying critical behaviour is the universality hypothesis, which is the observation that the behaviour of widely different systems on the microscopic scale can display identical behaviour in the critical region. This hypothesis is supported by large amounts of empirical evidence, and is also motivated further by Wilson's theory of the renormalization group[12]. In the following subsections a brief review of some aspects of critical phenomena will be given.

2.2.1 Critical Exponents and Scaling

At a critical point the free energy f of a system becomes singular. For the d-dimensional Ising model in an external field the free energy depends on two parameters, the temperature T and the external field strength H. It follows from the renormalization group that the singular part of the free energy f_s varies with a change of scale λ as

$$f_s\left(t, h\right) = \lambda^{-d} f_s\left(\lambda^{y_t} t, \lambda^{y_h} h\right), \tag{2.6}$$

where $t = \frac{T - T_c}{T_c}$ and $h = H - H_c$. From this scaling relation the behavior of various thermodynamic quantities, such as the magnetization m and specific heat c, by appropriately differentiating the free energy. For instance setting $h = 0$ and $\lambda = |t|^{-\frac{1}{y_t}}$ leads to

$$m\left(t, 0\right) = \left(-t\right)^{\beta} m\left(-1, 0\right), \tag{2.7}$$

$$c\left(t, 0\right) = |t|^{-\alpha} C\left(\pm 1, 0\right), \tag{2.8}$$

where $\alpha = \frac{2y_t - d}{y_t}$ and $\beta = \frac{d - y_h}{y_t}$ are referred to as critical exponents. Another important scaling relation is for the correlation length ξ and is given by

$$\xi \sim |t|^{-\nu} \tag{2.9}$$

Critical behaviour of other thermodynamic quantities can be derived similarly and will have their own critical exponents, but due to the scaling form (2.6) all the exponents are related to each other through y_t and y_h in what is called scaling laws. Historically it had already been noted from empirics that critical exponents seemed to be related to each other even before the introduction of the renormalization group.

2.2.2 Finite Size Scaling

A profound realization is that it is impossible in theory for a system of finite size to undergo a phase transition[12, 13]. For sufficiently large systems as in experiments we still do observe phase transitions for all intents and purposes. In simulations systems are however very small in comparison to experiments, and thoroughly understanding the effects of finite sizes becomes important. A notable finite size effect is the disappearance of divergences in thermodynamic quantities.

Considering the specific heat which has the infinite size scaling given by (2.8) the finite size is accounted for by postulating a finite size scaling function $\tilde{c}$ as[12]

$$c\left(t, 0\right) = |t|^{-\alpha} \tilde{c}\left(\frac{L}{\xi\left(t\right)}\right), \tag{2.10}$$

where $\tilde{c}\left(x\right)$ has two particular limits. For $x \to \infty$ the function $\tilde{c}\left(x\right) \to \text{const.}$, while when $x \to 0$ the function $\tilde{c}\left(x\right) \to x^{\alpha/\nu}$. The first limit assures the original

scaling behaviour for the infinite system, while the second limit removes the singular behaviour for finite systems since the factor $|t|^{-\alpha}$ is cancelled by $\tilde{c}(x)$. A further remark is that for a quantity $Q(t, L)$ that scales in the infinite size limit as $|t|^{y}$ the quantity

$$L^{y/\nu}Q(t, L) = \left(L^{1/\nu}|t|\right)^{y} \varphi\left(L^{1/\nu}|t|\right) \tag{2.11}$$

where it may be noted that the right hand side is only dependent of $L^{1/\nu}|t|$. Plotting the left hand side of (2.11) against $L^{1/\nu}|t|$ produces the same curve independently of the actual system size L, such that data from different system sizes collapses onto each other.

One particular quantity relevant to this thesis is the so called Binder cumulant[14] defined here as

$$g = \frac{1}{2}\left(3 - \frac{\langle m^4 \rangle}{\langle m^2 \rangle^2}\right). \tag{2.12}$$

The definition of the Binder cumulant varies somewhat between authors, but the important part is the ratio of the fourth and second moments of m. Using the definition (2.12) the Binder cumulant for an infinite Ising system follows

$$g = \begin{cases} 1, & T < T_c, \\ 0, & T > T_c. \end{cases} \tag{2.13}$$

Furthermore for finite systems the Binder cumulant typically scales as

$$g = \tilde{g}\left(L^{1/\nu}t\right), \tag{2.14}$$

and as such only depends on $L^{1/\nu}t$. In Sec. 2.6 the scaling form for the Binder cumulant of a quantum Ising system is shown.

2.3   Random Transverse Field Quantum Ising Model

The Ising model is a well studied system within statistical mechanics. It describes a very simple magnetic system defined on the sites of a lattice. In its simplest form its behaviour is determined by the Hamiltonian given by

$$H = -J\sum_{\langle ij \rangle} s_i s_j, \tag{2.15}$$

where J is the coupling strength and s_i are the spins in the lattice and may only take values $s_i = \pm 1$. As is conventional $\langle ij \rangle$ denotes that the indices in the sum are chosen such that only pairs of nearest neighbors contribute to H. The model can be generalized in many ways, such as by adding longer ranged interactions or by

adding many body interactions e.g. $Js_is_js_k$. Another generalization to the model is by having the coupling strength depend on the lattice index. Spin glasses are an example of a class of systems belonging to this type of generalization. In a spin glass the couplings are randomly assigned in the lattice, which under certain circumstances result in what is known as frustation, i.e. the ground state of the system (the state which minimizes H) is not unique.

Within quantum physics there is an analogy to the Ising model, and its dynamics are governed by the Hamilton operator $\hat{\mathcal{H}}$ given by

$$\hat{\mathcal{H}} = -J \sum_{\langle ij \rangle} \hat{\sigma}_i^z \hat{\sigma}_j^z, \tag{2.16}$$

where $\hat{\sigma}_i^z$ is the z direction Pauli matrix acting on the i:th spin in the lattice. This model may be generalized in the same ways as the classical model, but the quantum nature also allows for additional generalizations. One notable example is the addition of a transverse field, which produces a Hamiltonian in the form

$$\hat{\mathcal{H}} = -J \sum_{\langle ij \rangle} \hat{\sigma}_i^z \hat{\sigma}_j^z - h \sum_i \hat{\sigma}_i^x, \tag{2.17}$$

where $\hat{\sigma}_i^x$ is the Pauli matrix in the x direction. The transverse field quantum Ising model experiences a phase transition at $T = 0$ as a function of the transverse field. Phase transitions of this kind are unique to quantum systems and arise due to quantum fluctuations which occur even in the absence of thermal fluctuations, i.e. when $T = 0$.

In this thesis a version of the one-dimensional quantum Ising model with random couplings and random transverse field is studied. The Hamilton operator for this model is

$$\hat{\mathcal{H}} = -\sum_i J_i \hat{\sigma}_i^z \hat{\sigma}_{i+1}^z - \sum_i h_i \hat{\sigma}_i^x. \tag{2.18}$$

The couplings and fields are random variables drawn from two distributions. Periodic boundary condition is applied, such that for a system of N spins $\hat{\sigma}_{N+1}^\alpha = \hat{\sigma}_1^\alpha$.

2.4 Quantum to Classical Mapping of the Ising Model

There are many efficient methods for numerically studying classical statistical mechanical systems. These methods are often not directly applicable to quantum statistical mechanics, however as was shown by Suzuki[4] it is possible to map certain quantum systems onto classical systems. The advantage of this mapping is that it allows the statistical mechanics of the quantum system to be studied with the numerical schemes developed for classical systems. This is indeed possible for the system described by (2.18). Readers familiar with the path integral formalism

may recognize aspects of the mapping, and when applied for the purposes of Monte Carlo simulations it is sometimes known as the path integral Monte Carlo method. The derivation of this mapping will be discussed below. It will be performed for a two spin system for simplicity, but the generalization is trivial, both for higher dimension and more spins.

The Hamiltonian for the two spin quantum system is

$$\hat{\mathcal{H}} = -J_1\hat{\sigma}_1^z\hat{\sigma}_2^z - h_1\hat{\sigma}_1^x - J_2\hat{\sigma}_2^z\hat{\sigma}_1^z - h_2\hat{\sigma}_2^x, \tag{2.19}$$

which gives the partition function as

$$Z = \sum_{\{s_1^0\}}\sum_{\{s_2^0\}} \left\langle s_1^0 s_2^0 \right| e^{-\beta\hat{\mathcal{H}}} \left| s_1^0 s_2^0 \right\rangle. \tag{2.20}$$

The sum $\sum_{\{s_1^0\}}$ denotes summation over all possible spin configurations for spin s_1^0. It can be argued that the second coupling term of (2.19) is unnecessary. While true for the two spin system it has still been included as it makes the generalization to more spins more directly apparent. Now introduce a shorthand notation for this sum as $\sum_{\{s_i^0\}} = \sum_{\{s_1^0\}}\sum_{\{s_2^0\}}$. The reason for the superindex 0 becomes clear below. The exponential function of a sum of operators $\sum_i \hat{A}_i$ can be decomposed into a product of operator exponentials by the Trotter formula[15]

$$e^{\sum_{i=1}^N \hat{A}_i} = \lim_{M\to\infty}\left(\prod_{i=1}^N e^{\frac{1}{M}\hat{A}_i}\right)^M = \lim_{M\to\infty}\prod_{k=1}^M\prod_{i=1}^N e^{\frac{1}{M}\hat{A}_i}. \tag{2.21}$$

The partition function may thereby be approximated by

$$Z_{L_\tau} = \sum_{\{s_i\}} \left\langle s_1^0 s_2^0 \right| \left(\prod_{k=1}^{L_\tau} e^{K_1\hat{\sigma}_1^z\hat{\sigma}_2^z} e^{K_2\hat{\sigma}_2^z\hat{\sigma}_1^z} e^{\tilde{h}_1\hat{\sigma}_1^x} e^{\tilde{h}_2\hat{\sigma}_2^x}\right) \left| s_1^0 s_2^0 \right\rangle, \tag{2.22}$$

where $K_i = \frac{\beta}{L_\tau}J_i$, and $\tilde{h}_i = \frac{\beta}{L_\tau}h_i$. In (2.22) the integer M has been relabeled as L_τ. Next use the completeness relation given by

$$\sum_{\{s_i\}} |s_1 s_2\rangle \langle s_1 s_2| = I, \tag{2.23}$$

where the vectors $|s_i\rangle$ constitute an orthonormal basis for the operator $\hat{\sigma}_1^z \hat{\sigma}_2^z$. Inserting $L_\tau - 1$ completeness relations yields

$$
\begin{aligned}
Z_{L_\tau} = \sum_{\{s_i^0\}} & \left\langle s_1^0 s_2^0 \right| e^{K_1 \hat{\sigma}_1^z \hat{\sigma}_2^z} e^{K_2 \hat{\sigma}_1^z \hat{\sigma}_2^z} e^{\tilde{h}_1 \hat{\sigma}_1^x} e^{\tilde{h}_2 \hat{\sigma}_2^x} \\
\times & \sum_{\{s_i^1\}} \left| s_1^1 s_2^1 \right\rangle \left\langle s_1^1 s_2^1 \right| e^{K_1 \hat{\sigma}_1^z \hat{\sigma}_2^z} e^{K_2 \hat{\sigma}_1^z \hat{\sigma}_2^z} e^{\tilde{h}_1 \hat{\sigma}_1^x} e^{\tilde{h}_2 \hat{\sigma}_2^x} \\
\times & \quad \cdots \\
\times & \sum_{\{s_i^{L_\tau - 1}\}} \left| s_1^{L_\tau - 1} s_2^{L_\tau - 1} \right\rangle \left\langle s_1^{L_\tau - 1} s_2^{L_\tau - 1} \right| e^{K_1 \hat{\sigma}_1^z \hat{\sigma}_2^z} e^{K_2 \hat{\sigma}_1^z \hat{\sigma}_2^z} e^{\tilde{h}_1 \hat{\sigma}_1^x} e^{\tilde{h}_2 \hat{\sigma}_2^x} \left| s_1^0 s_2^0 \right\rangle
\end{aligned}
$$
$$(2.24)$$

which can be rewritten as

$$
Z_{L_\tau} = \sum_{\{s_i^0\}} \cdots \sum_{\{s_i^{L_\tau - 1}\}} \left(\prod_{k=0}^{L_\tau - 1} \left\langle s_1^k s_2^k \right| e^{K_1 \hat{\sigma}_1^z \hat{\sigma}_2^z} e^{K_2 \hat{\sigma}_2^z \hat{\sigma}_1^z} e^{\tilde{h}_1 \hat{\sigma}_1^x} e^{\tilde{h}_2 \hat{\sigma}_2^x} \left| s_1^{k+1} s_2^{k+1} \right\rangle \right),
$$
$$(2.25)$$

where the last factor $\left| s_1^{L_\tau} s_2^{L_\tau} \right\rangle = \left| s_1^0 s_2^0 \right\rangle$. Now introduce another shorthand for the sums $\sum_{\{s_i^k\}} = \sum_{\{s_i^0\}} \cdots \sum_{\{s_i^{L_\tau - 1}\}}$. Furthermore the operators $e^{K_i \hat{\sigma}_i^z \hat{\sigma}_{i+1}^z}$ are diagonal in the basis $|s_1^k s_2^k\rangle$, and thus it is possible to write

$$
Z_{L_\tau} = \sum_{\{s_i^k\}} \left(\prod_{k=0}^{L_\tau - 1} e^{K_1 s_1^k s_2^k} e^{K_2 s_1^k s_2^k} \left\langle s_1^k s_2^k \right| e^{\tilde{h}_1 \hat{\sigma}_1^x} e^{\tilde{h}_2 \hat{\sigma}_2^x} \left| s_1^{k+1} s_2^{k+1} \right\rangle \right).
$$
$$(2.26)$$

The operator $e^{\tilde{h}_i \hat{\sigma}_i^x}$ only operates on the $|s_i^k\rangle$ part of $|s_1^k s_2^k\rangle$ and so

$$
Z_{L_\tau} = \sum_{\{s_i^k\}} \left(\prod_{k=0}^{L_\tau - 1} e^{K_1 s_1^k s_2^k} e^{K_2 s_1^k s_2^k} \left\langle s_1^k \right| e^{\tilde{h}_1 \hat{\sigma}_1^x} \left| s_1^{k+1} \right\rangle \left\langle s_2^k \right| e^{\tilde{h}_2 \hat{\sigma}_2^x} \left| s_2^{k+1} \right\rangle \right).
$$
$$(2.27)$$

The matrix elements

$$
T\left(s_i^k, s_i^{k+1} \right) = \left\langle s_i^k \right| e^{\tilde{h}_i \hat{\sigma}_i^x} \left| s_i^{k+1} \right\rangle
$$
$$(2.28)$$

can be rewritten into a more convenient form. First it should be noted that the exponential operator is diagonal when expressed in $|s_i^x\rangle$, the eigenstates of $\hat{\sigma}_i^x$, that is to say

$$
e^{\tilde{h}_i \hat{\sigma}_i^x} = \sum_{s_i^x = \pm 1} |s_i^x\rangle e^{\tilde{h}_i s_i^x} \langle s_i^x|.
$$
$$(2.29)$$

Next the various inner products between the eigenstates of $\hat{\sigma}_i^x$ and $\hat{\sigma}_i^z$ are given by

$$\left\langle s_i^k = +1 | s_i^x = +1 \right\rangle = \frac{1}{\sqrt{2}} \qquad\qquad \left\langle s_i^k = +1 | s_i^x = -1 \right\rangle = \frac{1}{\sqrt{2}}$$

$$\left\langle s_i^k = -1 | s_i^x = +1 \right\rangle = \frac{1}{\sqrt{2}} \qquad\qquad \left\langle s_i^k = -1 | s_i^x = -1 \right\rangle = -\frac{1}{\sqrt{2}}$$

Thus the matrix elements become

$$T\left(s_i^k, s_i^{k+1}\right) = \left\langle s_i^k | s_i^x = +1 \right\rangle e^{\tilde{h}_i} \left\langle s_i^x = +1 | s_i^{k+1} \right\rangle + \left\langle s_i^k | s_i^x = -1 \right\rangle e^{-\tilde{h}_i} \left\langle s_i^x = -1 | s_i^{k+1} \right\rangle. \tag{2.30}$$

Particularly

$$\left\langle s_i^k | s_i^x = +1 \right\rangle e^{\tilde{h}_i} \left\langle s_i^x = +1 | s_i^{k+1} \right\rangle = \frac{1}{2} e^{\tilde{h}_i} \tag{2.31}$$

independently of the values s_i^k and s_i^{k+1}, while

$$\left\langle s_i^k | s_i^x = -1 \right\rangle e^{-\tilde{h}_i} \left\langle s_i^x = -1 | s_i^{k+1} \right\rangle = \begin{cases} +\frac{1}{2} e^{-\tilde{h}_i}, & s_i^k = s_i^{k+1} \\ -\frac{1}{2} e^{-\tilde{h}_i}, & s_i^k = -s_i^{k+1} \end{cases} \tag{2.32}$$

and thus

$$T\left(s_i^k, s_i^{k+1}\right) = \begin{cases} \cosh(\tilde{h}_i), & s_i^k = s_i^{k+1} \\ \sinh(\tilde{h}_i), & s_i^k = -s_i^{k+1} \end{cases} \tag{2.33}$$

It would be more practical if $T\left(s_i^k, s_i^{k+1}\right)$ could be written without distinguishing the two cases explicitly. One such way would be to write $T\left(s_i^k, s_i^{k+1}\right)$ instead as

$$T\left(s_i^k, s_i^{k+1}\right) = \frac{1}{2}\left(e^{\tilde{h}_i} + s_i^k s_i^{k+1} e^{-\tilde{h}_i}\right). \tag{2.34}$$

This form is not very useful in practice however. Instead a different form is proposed as

$$T\left(s_i^k, s_i^{k+1}\right) = e^{A_i + H_i s_i^k s_i^{k+1}}, \tag{2.35}$$

where A_i and H_i are constants. Comparison with (2.33) gives

$$e^{A_i + H_i} = \cosh(\tilde{h}_i),$$
$$e^{A_i - H_i} = \sinh(\tilde{h}_i), \tag{2.36}$$

or

$$A_i + H_i = \ln\left(\cosh(\tilde{h}_i)\right), \tag{2.37}$$

$$A_i - H_i = \ln\left(\sinh(\tilde{h}_i)\right). \tag{2.38}$$

Solving for H_i and A_i we get

$$H_i = \frac{1}{2} \ln \left(\frac{\cosh(\tilde{h}_i)}{\sinh(\tilde{h}_i)} \right) = \frac{1}{2} \ln \left(\coth(\tilde{h}_i) \right) \tag{2.39}$$

$$A_i = \frac{1}{2} \ln \left(\cosh(\tilde{h}_i) \sinh(\tilde{h}_i) \right) = \frac{1}{2} \ln \left(\frac{1}{2} \sinh(2\tilde{h}_i) \right) \tag{2.40}$$

Thus if H_i and A_i are chosen according to (2.39) and (2.40) the form of $T\left(s_i^k, s_i^{k+1}\right)$ given by (2.35) holds. Inserting this form of $T\left(s_i^k, s_i^{k+1}\right)$ into (2.27) yields

$$Z_{L_\tau} = \sum_{\{s_i^k\}} \left(\prod_{k=0}^{L_\tau - 1} e^{A_1 + A_2} e^{K_1 s_1^k s_2^k} e^{K_2 s_1^k s_2^k} e^{H_1 s_1^k s_1^{k+1}} e^{H_2 s_2^k s_2^{k+1}} \right), \tag{2.41}$$

which ultimately can be rewritten by combining all the exponential functions

$$Z_{L_\tau} = \sum_{\{s_i^k\}} C \exp \left(\sum_{i,k} \left(K_i s_i^k s_{i+1}^k + H_i s_i^k s_i^{k+1} \right) \right), \tag{2.42}$$

where $C = \exp\left(\sum_i A_i\right)$ is a effectively irrelevant constant. The sums over i goes over all the spins, for this example $i = 1, 2$, while k takes values $k = 0, 1, \ldots, L_\tau - 1$. This partition function for the one dimensional quantum Ising system is equivalent to the partition function of the two dimensional classical Ising system.

It should be noted that while the derivation presented here was done for a two spin extending the derivation to the general case of N spins is trivial, and (2.42) has the same form, except that $i = 1, 2, \ldots, N$. This derivation can also be done for quantum systems in higher dimension and in general a quantum system in d dimensions maps to a classical system in $d + 1$ dimensions. In the following the introduced dimension will be referred to as the Trotter direction or the τ direction, while the original dimension of the system will be referred to as the x direction, or the spatial direction.

2.5 Aspects of the Quantum to Classical Mapping

From the partition function (2.42) it is possible to identify an effective Hamiltonian of the two-dimensional model as

$$\beta_{\text{eff}} H_{\text{eff}} = \sum_{i,k} \left(K_i s_i^k s_{i+1}^k + H_i s_i^k s_i^{k+1} \right). \tag{2.43}$$

Here an effective classical temperature T_{eff} and inverse temperature $\beta_{\text{eff}} = 1/T_{\text{eff}}$ have been introduced to mimic the classical partition funciton of a two-dimensional

Ising model, but it should not be confused with the actual temperature of the quantum system. The quantum phase transition of an N spin system is probed by adjusting the ratio of the average of the couplings $\bar{J} = \frac{1}{N}\sum_{i=1}^{N} J_i$ to the fields $\bar{h} = \frac{1}{N}\sum_{i=1}^{N} h_i$ of the quantum system to some critical value. When the ratio

$$\frac{\bar{h}}{\bar{J}} \tag{2.44}$$

is large the system is in a disordered, paramagnetic state, while when it is small the system is in an ordered, ferromagnetic state. This ratio can be adjusted by adjusting the distributions of the parameters J_i and h_i of the quantum system.

However, in practice it is more convenient to work directly with the effective parameters. The ratio (2.44) can be adjusted by letting the K_i and H_i be drawn from two fixed distributions and varying the effective temperature T_{eff} instead. Thereby the effective temperature acts in a sense as the field and in the following sections T_{eff} will be denoted simply by T and referred to as the field unless otherwise stated. In Fig. 2.1 the behaviour of the parameters J and h of the non-disordered quantum system is illustrated to show how the ratio of the fields and couplings are varied by varying T. By introducing this effective temperature simulations can be done completely analogously with the numerical simulations of the classical Ising model, although the physical interpretation of T is more abstract.
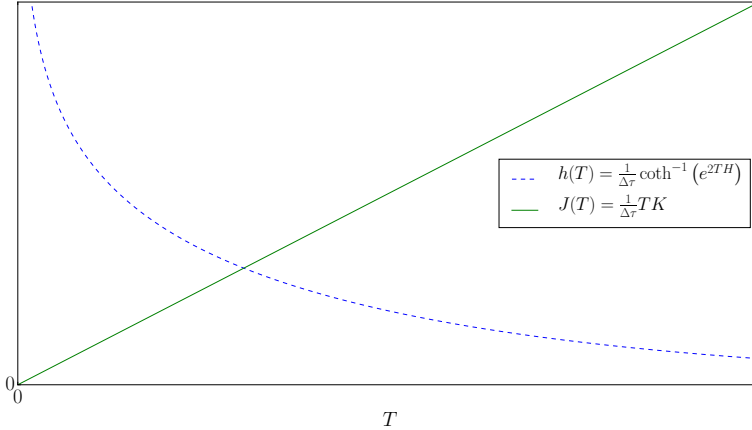

Figure 2.1. Illustration of the coupling J and field h of the quantum system behaves as the effective temperature T is increased for some conveniently chosen values of H, K and $\Delta\tau = \beta/L_\tau$.

The for this thesis the distributions for the two types of couplings K_i and H_i in the effective model are

$$\rho\left(K\right) = \begin{cases} 1, & 1 \geq K \geq 0, \\ 0, & \text{otherwise,} \end{cases} \tag{2.45}$$

$$\pi\left(H\right) = \begin{cases} 2e^{-2H}, & H \geq 0, \\ 0, & \text{otherwise.} \end{cases} \tag{2.46}$$

Another consequence of the quantum to classical mapping is the ratio

$$\Delta\tau = \frac{\beta}{L_\tau}, \tag{2.47}$$

where $\Delta\tau$ is determined, by the system size L_τ in the τ direction and β. By fixing the $\Delta\tau$ a relation between the inverse temperature of the quantum system and the size of the classical system in the τ direction is established. In this thesis $\Delta\tau = 1$ has been used such that

$$L_\tau = \beta. \tag{2.48}$$

Hence the L_τ will be referred to in the following as inverse temperature.

2.6 Analytical Results

Disordered systems are complicated to study. Analytical solutions in statistical mechanics are rare, and when the system involves disorder even numerical study becomes difficult, since in order to understand the overall properties of the disordered system many different realizations of the system must be observed. It is not enough to simply perform one in thorough simulatin of a single realization. In 1992 D. Fisher[8, 9] demonstrated how various analytical results could be determined for the system described by (2.18) using a renormalization group approach. The results are independent of the distributions of J_i and h_i.

Among the predictions were that the system experiences what is known as activated dynamic scaling. This activated dynamic scaling can be observed for instance in the Binder cumulant g as its scaling function becomes

$$g = \tilde{g}\left(L^{1/\nu}t, \frac{L_\tau}{e^{kL^z}}\right), \tag{2.49}$$

where k is a constant. The term activated dynamic scaling refers to the ratio between L_τ and e^{kL^z}, which stands in contrast to e.g. the ordered model where the scaling function is instead[5]

$$g = \tilde{g}\left(L^{1/\nu}t, \frac{L_\tau}{L^z}\right). \tag{2.50}$$

The exponent z of (2.49) was determined by Fisher to be $z = 1/2$.

Another prediction was the differing behaviour in the scaling of the typical and average correlation functions. The typical correlation function scales as

$$C_{\text{typ}}\left(r\right) \sim e^{-kr^{1/2}}, \tag{2.51}$$

where k is a constant. On the other hand the average correlation scales as

$$C_{\text{av}}\left(r\right) \sim r^{\varphi-2}, \tag{2.52}$$

where $\varphi = \frac{1+\sqrt{5}}{2}$ is the golden ratio.

Chapter 3

Numerical Analysis Methods

In the following chapter the numerical aspects of the thesis are described. First an introduction is given to the theory of Markov chain Monte Carlo methods for simulating physics in statistical mechanics. Two specific algorithms which have been used during the work of this thesis, the Metropolis and the Wolff algorithms, are described. Furthermore the method of histogram extrapolation is detailed. Next some methods for estimating the statistical errors which always accompany Monte Carlo methods are reviewed. This is followed by a brief discussion of pseudorandom numbers. Finally some implementation details are given.

3.1   Markov Chain Monte Carlo Methods

In this section the basics of Markov chain Monte Carlo simulations will be briefly presented. For a more detailed review of the subject see for instance Newman and Barkema[16].

As was argued in Sec. 2.1, knowing the partition function one has access to many properties of the system. In practice it is often very difficult to find an analytic expression for the partition function.

A different approach to the problem of determining the macroscopic properties is by computing the expectations directly. The expectation of some quantity $X(\omega)$ can be estimated from a set of N sample states $\{\omega_n\}$, where each state is drawn with a corresponding probability p_n. The best estimate of the expectation is given by

$$\langle X \rangle \approx \frac{\sum_{n=1}^{N} X(\omega_n) \, p_n^{-1} e^{-\beta H(\omega_n)}}{\sum_{n=1}^{N} p_n^{-1} e^{-\beta H(\omega_n)}}. \tag{3.1}$$

If the states can be drawn directly from the Boltzmann distribution then the estimator (3.1) becomes

$$\langle X \rangle \approx \bar{X} = \frac{1}{N} \sum_{n=1}^{N} X(\omega_n), \tag{3.2}$$

i.e. the arithmetic mean.

Markov chain Monte Carlo methods utilize Markov chains to produce sample states according to a desired target distribution. A Markov chain in the context of Monte Carlo simulations in statistical physics is a sequence of states where each subsequent state is generated solely from its immediate predecessor. The way in which a new state is generated from the previous is what defines a specific Monte Carlo method.

A way of measuring time in Monte Carlo simulations of spin systems is by counting the number of attempts at flipping spins. Most commonly time is measured in sweeps, which corresponds to a number of attempts equal to the system size. For a 4×4 lattice of spins a sweep is equal to 16 attempts. Whenever the word sweep is used in this thesis this is what is meant.

If a proper method is used the system may be initialized to an arbitrary state. Then the system is evolved using the method from the arbitrary state for a number of sweeps without taking any measurement. This is done because the intially generated states will not necessarily be correctly distributed, due to correlations to the arbitrary initial state. This procedure is called the warmup, burn-in or equilibration phase. It is often necessary to study the time it takes for the system to equilibrate, so that systematic errors due to initial configuration are avoided.

In order for the states generated to be Boltzmann distributed the generating method should obey two conditions. The transitions between states should obey detailed balance, and it should be ergodic.

3.1.1 Detailed Balance

Detailed balance is defined by

$$R(\omega_n \to \omega_m) P(\omega_m) = R(\omega_m \to \omega_n) P(\omega_n), \tag{3.3}$$

where $R(\omega_n \to \omega_m)$ is the probability of transition from state ω_n to state ω_m, and $P(\omega_n)$ is the probability of the system being in state ω_n, which here is the Boltzmann distribution. Rearranging this condition produces

$$\frac{R(\omega_n \to \omega_m)}{R(\omega_m \to \omega_n)} = \frac{P(\omega_m)}{P(\omega_n)} = e^{-\beta(H(\omega_m) - H(\omega_n))}, \tag{3.4}$$

which is the condition for transitions between states in order to generate the Boltzmann distribution.

3.1.2 Ergodicity

A system in statistical mechanics is said to be ergodic if it will traverse its entire state space given sufficient time. In other words this means that it should not be completely locked into a subregion of the state space. For a Markov chain to be ergodic it should be possible for it to reach each of the states in a finite number of steps. If the transition rate to and from a certain state ω_n is 0 for all states expect ω_n itself, then the algorithm would not be ergodic.

Thus as long as condition (3.4) is satisfied and the algorithm is sure to be ergodic it will sample states with proper distribution. These conditions are sufficiently loose that they allow for many ways of generating Boltzmann distributed states.

3.1.3 Selection and Acceptance Ratios

The ratio (3.4) is what restricts the transition probabilities for each pair of states, but it allows for a lot of freedom in how the probabilities are chosen. An important note is that the transition from one state to itself

$$R\left(\omega_n \rightarrow \omega_n\right) \neq 0 \tag{3.5}$$

in general. Thereby it is possible to decompose the transition probabilities into

$$R\left(\omega_n \rightarrow \omega_m\right) = S\left(\omega_n \rightarrow \omega_m\right) A\left(\omega_n \rightarrow \omega_m\right), \tag{3.6}$$

where we call $S\left(\omega_n \rightarrow \omega_m\right)$ the selection probability, and $A\left(\omega_n \rightarrow \omega_m\right)$ the acceptance probability. The selection probability serves to select a state ω_m to be the next state given a current state ω_n. The acceptance probability then represents the probability of actually performing the transition to ω_m rather than just remaining in the current state ω_n. The original ratio (3.4) then becomes

$$\frac{S\left(\omega_n \rightarrow \omega_m\right)}{S\left(\omega_m \rightarrow \omega_n\right)} \cdot \frac{A\left(\omega_n \rightarrow \omega_m\right)}{A\left(\omega_m \rightarrow \omega_n\right)} = e^{-\beta(H(\omega_m)-H(\omega_n))}. \tag{3.7}$$

The decomposition (3.6) leaves the method for selecting new states rather unrestricted, as long as ergodicity is respected and the rates of accepting the generated states are adjusted to maintain detailed balance.

However it should be noted that if the acceptance probabilities are low the same state will be sampled many times, and the state space will be explored very slowly. A good Markov chain Monte Carlo method is therefore usually one with high probabilities of acceptance.

3.2 Metropolis algorithm

One of the more ubiquitous Markov chain Monte Carlo methods is the Metropolis-Hastings algorithm[17]. A special case of the Metropolis-Hastings algorithm is

known simply as the Metropolis algorithm and it is defined by that the selection probabilities are symmetric, i.e.

$$S\left(\omega_n \to \omega_m\right) = S\left(\omega_m \to \omega_n\right). \tag{3.8}$$

This leads to an acceptance ratio of

$$\frac{A\left(\omega_n \to \omega_m\right)}{A\left(\omega_m \to \omega_n\right)} = e^{-\beta(H(\omega_m)-H(\omega_n))}. \tag{3.9}$$

In order to maximize the acceptance probabilities we may set one of the probabilities to 1, which maximizes both probabilities. This gives acceptance probabilities as

$$A\left(\omega_n \to \omega_m\right) = \begin{cases} 1 & \text{if } H\left(\omega_n\right) > H\left(\omega_m\right), \\ e^{-\beta(H(\omega_m)-H(\omega_n))} & \text{otherwise.} \end{cases} \tag{3.10}$$

This way the ratio of acceptance rates is correct simultaneously as the acceptance probabilities are maximized. A common choice of selection probabilities for spin systems such as the Ising model is to set uniform probability for all states that differ from the previous state only in the value of one of the spins.

While the Metropolis algorithm is elegant in its simplicity it has issues. The algorithm tends to struggle near the temperature of a phase transition, where the generated states become highly correlated. This effect is known as critical slowing down, and is a result of the fact that the system fluctuates on all scales. Single spin flip algorithms generally give long correlation times that makes convergence slow, typically at $t_{\text{corr}} \sim L^2$ where L is the system size.

3.3   Wolff Cluster Algorithm

The problem of critical slowing down of the Metropolis algorithm can be avoided by a change of algorithm. Another Markov chain Monte Carlo method is the Wolff cluster algorithm[18], which is significantly less affected by the critical slowing down. Rather than changing the system state one spin at a time the algorithm starts by selecting a seed spin, generates a cluster of spins, and flips them simultaneously.

Consider a two-dimensional Ising model with site dependent couplings J_{ij} between neighboring spins at sites i and j. The Wolff algorithm goes as follows:

1. Pick the seed spin at random from the lattice. This is added to a list representing the cluster to be flipped.

2. For each neighbor of the spin just added to the cluster compare the spin values. If the neighbor has the same spin value, add it to a list of neighbors, otherwise do nothing.

3. If the neighbor list is empty advance to step 6. Otherwise remove the first spin of the neighbor list from the list, and perform a test for if it should be added to the cluster. The test should be performed such that the probability of accepting the spin into the cluster is $p_{ij} = 1 - e^{-2\beta J_{ij}}$.

4. If the spin is added to the cluster, repeat from step 2.

5. If the spin is not added, repeat from step 3.

6. Flip the cluster. Repeat from step 1.

The algorithm is ergodic, it is always possible for all neighbors to be rejected to the cluster such that the algorithm may flip just a single spin. By performing at most as many flips as there are spins in the system any state can be reached.

For the condition of detailed balance we consider an arbitrary cluster containing some number of spins. We recall the detailed balance equation as

$$\frac{S\left(\omega_n \to \omega_m\right) A\left(\omega_n \to \omega_m\right)}{S\left(\omega_m \to \omega_n\right) A\left(\omega_m \to \omega_n\right)} = e^{-\beta(H(\omega_m)-H(\omega_n))} \tag{3.11}$$

The change in energy from state ω_n to state ω_m is given by the difference in number of bonds that are changed from antiparallel to parallel (contributing to lower the energy) and the number of bonds which are changed from parallel to antiparallel (contributing to a higher energy). The only bonds that change are the bonds along the border of the cluster. Inside the cluster the spins are aligned as they were before the flip relative to each other, and the same goes for the spins outside the cluster. The contribution to the energy change from an antiparallel-to-parallel bond flip corresponds to $-2J_{ij}$ and for parallel-to-antiparallel corresponds to $2J_{ij}$, where i and j denote between which two spins the bond is. Thus the change in energy

$$\Delta H_{\omega_n \to \omega_m} \equiv H\left(\omega_m\right) - H\left(\omega_n\right) = -2\left(\sum_{ij\in\Lambda_-} J_{ij} - \sum_{kl\in\Lambda_+} J_{kl}\right) \tag{3.12}$$

where Λ_+ denotes the indices of pairs of spins where the bond changes from parallel to antiparallel resulting in an increased energy, and Λ_- denotes indices of spins where the bond changes from parallel to antiparallel, thus contributing to lower the energy. The right hand side is thus

$$e^{-\beta\Delta H_{\omega_n \to \omega_m}} = \frac{\prod_{ij\in\Lambda_-} e^{2\beta J_{ij}}}{\prod_{kl\in\Lambda_+} e^{2\beta J_{kl}}}. \tag{3.13}$$

Next we turn to the ratio between the selection probabilities. The probability of selecting a particular cluster is given by the product of the probabilities of adding each spin in the cluster to it, and the probabilities of not adding the spins parallel with the cluster along the border of the cluster.

The probability of adding each spin in the cluster to the cluster is the same irregardles of which direction the transition occurs. Each spin in the cluster is equally likely to be chosen as seed, and all the subsequent spins added are added with the same probability both ways. This factor thereby cancel out in the numerator and the denominator of (3.11). The only difference in the selection rates of the two directions is due to the difference in which spins are parallel to the cluster along the perimeter of the cluster. Incidentally, the spins which are parallel with the cluster before the flips are exactly the spins indicated by Λ_+. The full probability of not adding every parallel spin along the perimeter of a given cluster in the transition $\omega_n \to \omega_m$ is

$$S\left(\omega_n \to \omega_m\right) \propto \prod_{ij \in \Lambda_+} \left(1 - \left(1 - e^{-2\beta J_{ij}}\right)\right) = \prod_{ij \in \Lambda_+} e^{-2\beta J_{ij}} \tag{3.14}$$

For the inverse transition $\omega_m \to \omega_n$ the parallel perimeter spins are the spins which where antiparallel to the cluster for the transition $\omega_n \to \omega_m$, and are indicated by Λ_- from before, and so

$$S\left(\omega_m \to \omega_n\right) \propto \prod_{ij \in \Lambda_-} e^{-2\beta J_{ij}}. \tag{3.15}$$

The ratio of the selection rates are now given by

$$\frac{S\left(\omega_n \to \omega_m\right)}{S\left(\omega_m \to \omega_n\right)} = \frac{\prod_{ij \in \Lambda_-} e^{2\beta J_{ij}}}{\prod_{ij \in \Lambda_+} e^{2\beta J_{ij}}} = e^{-\beta \Delta H_{\omega_n \to \omega_m}}. \tag{3.16}$$

With these selection rates the ratio between acceptance probabilities must be set to unity, and so the acceptance probabilities may be set to 1 both ways.

3.3.1   Improved Estimators

An additional advantage of using cluster algorithms such as the Wolff algorithm is that they offer efficient methods, so called improved estimators, for calculating various quantities of the system[16]. Here an improved estimator is used for the equal time spin-spin correlation function. Equal time implies that the two spins that are correlated share the same coordinate in the Trotter direction. In other words the separation of the spins is entirely along the x direction.

The improved estimator for a system of spatial size L is computed through the following steps:

- At the start of the measurement phase of a simulation a list with L entries, all set to 0 is created.

- When a seed spin is selected the zeroth element is incremented 1.

- Every time a spin is added to the cluster with the same coordinate value along the Trotter direction as the seed the nth element of the list is incremented, where the index n is defined as

$$n = \begin{cases} i_{\text{spin}} - i_{\text{seed}}, & i_{\text{spin}} > i_{\text{seed}}, \\ i_{\text{spin}} - i_{\text{seed}} + L, & i_{\text{spin}} < i_{\text{seed}}, \end{cases} \tag{3.17}$$

The indices i_{spin} and i_{seed} denote the spatial coordinates of the newly added spin and the seed spin respectively.

- At the end of the simulation each entry in the list is normalized by division by the number of clusters flipped in during the measurement of the correlation. By doing this the zeroth element always becomes 1.

Improved estimators generally are subject to less variance than direct estimators.

3.4 Histogram Extrapolation

A common tool in magnifying the amounts of data obtained from a single Monte Carlo simulation today is a technique called histogram extrapolation. It can for instance be used to extrapolate information about the system at a different temperature than the one at which the simulation runs.

The name is derived from the theoretical background where a two-dimensional histogram is constructed for the quantity being measured along with corresponding energies. This histogram is used to estimate the underlying (simultaneous) probability distribution, and subsequently the distribution at other temperatures is estimated by application of a transformation on the original distribution. In fact the transformation from the original distribution to another at a different temperature is exact. However, since the original distribution is only estimated by the histogram the method is plagued by statistical error. For temperatures where the two distributions overlap the statistical errors are small, but as the overlap decreases the error grows large.

In practice storing the full histogram is not often viable, however it is possible to perform the extrapolation directly without saving the histogram. The method is outlined in the following. Let ω denote one configuration of the system, and let Ω be the set of all possible configurations ω. Assume that the expectation of a quantity A, which is a function of the system configuration $A(\omega)$, is to be determined for the system at temperature β. First recalling that the defintion of the expectation $\langle A \rangle$ is

$$\langle A \rangle_\beta = \frac{\sum_{\omega \in \Omega} A(\omega) e^{-\beta H(\omega)}}{\sum_{\omega \in \Omega} e^{-\beta H(\omega)}}. \tag{3.18}$$

Now let β' be a temperature different from β and we have

$$
\begin{aligned}
\langle A \rangle_\beta &= \frac{\sum_{\omega \in \Omega} A\left(\omega\right) e^{-\beta H(\omega)} e^{-\beta' H(\omega)} e^{\beta' H(\omega)}}{\sum_{\omega \in \Omega} e^{-\beta H(\omega)} e^{-\beta' H(\omega)} e^{\beta' H(\omega)}} \cdot \frac{\sum_{\omega \in \Omega} e^{-\beta' H(\omega)}}{\sum_{\omega \in \Omega} e^{-\beta' H(\omega)}} \\
&= \frac{\sum_{\omega \in \Omega} A\left(\omega\right) e^{-\left(\beta - \beta'\right) H(\omega)} e^{-\beta' H(\omega)}}{\sum_{\omega \in \Omega} e^{-\beta' H(\omega)}} \Big/ \frac{\sum_{\omega \in \Omega} e^{-\left(\beta - \beta'\right) H(\omega)} e^{-\left(\beta - \beta'\right) H(\omega)}}{\sum_{\omega \in \Omega} e^{-\beta' H(\omega)}} \\
&= \frac{\left\langle A e^{-\left(\beta - \beta'\right) H} \right\rangle_{\beta'}}{\left\langle e^{-(\beta - \beta') H} \right\rangle_{\beta'}}.
\end{aligned}
\tag{3.19}
$$

In practice the numerator and denominator of (3.19) are estimated by their corresponding arithmetic means during a simulation run for a large set of different temperature values β.

3.5   Error estimation

Monte Carlo methods are statistical methods and are inherently affected by statistical errors. In order for the results obtained from such methods it is important to assess the magnitude of these errors. The methods used in this thesis are introduced here.

3.5.1   Standard Error of the Mean

A simple way of estimating the error in an average is by using the standard error of the mean formula. Given a sample $\{x_i\}$ of N data points drawn independently from the same distribution the average of the data points $\bar{x}$ has a distribution with standard deviation of

$$
\sigma_{\bar{x}} = \frac{\sigma}{\sqrt{N}},
\tag{3.20}
$$

where σ is the standard deviation of the distribution of the x_i. The error of the the observed average is estimated by this standard deviation $\sigma_{\bar{x}}$. Most often the exact standard deviation σ is not known for the distribution of x_i. In such cases it may be estimated by the sample standard deviation s given by

$$
s = \sqrt{\frac{1}{N-1} \sum_{i=1}^{N} \left(x_i - \bar{x}\right)^2},
\tag{3.21}
$$

and the error of the average is estimated by

$$
\sigma_{\bar{x}} \approx \frac{s}{\sqrt{N}}.
\tag{3.22}
$$

3.5.2 Propagation of Error Formula

In cases where a quantity x has an error σ_x which is known it is possible to estimate the error in a derived quantity y by the propagation of error formula. If y is derived from x by a differentiable mapping $f(x)$ the error in y is estimated by

$$\sigma_y = \frac{\partial f}{\partial x}\sigma_x. \tag{3.23}$$

3.5.3 Bootstrap Error Estimation

While (3.22) and (3.23) offer simple and practical error estimate for averages and differentiable functions, they are not applicable generally. In this thesis some quantities are determined by involved computations that are not easily analyzed for error. For instance maxima are computed for polynomials which are fitted from Monte Carlo averages. The averages carry with them errors which propagate to the locations of the maxima. A very general method for estimating error is the bootstrap method[19], which will be outlined in the following.

Suppose there is a sample $\{x_i\}$ of N data points and a quantity $\theta(\{x_i\})$ which is calculated from the sample. Now from the full set of data $\{x_i\}$ a new set $\{x_i'\}$ of N points are picked out at random. Some points of $\{x_i\}$ are selected multiple times, while others are not selected at all. From this new sample $\theta(\{x_i'\})$ is computed and stored. This procedure is repeated M times. When this is done the error in $\theta(\{x_i\})$ is estimated by the sample standard deviation of the set of generated $\theta(\{x_i'\})$

$$\sigma_\theta = \sqrt{\frac{1}{M-1}\sum_{j=1}^{M}\left(\theta_j - \bar{\theta}\right)^2}, \tag{3.24}$$

where θ_j denote the M generated samples, and $\bar{\theta}$ is the average of these generated samples.

3.6 Pseudorandom Number Generation

The Monte Carlo algorithms are heavily reliant on random numbers. Nature provides few easily accessible sources of true randomness, but fortunately it is still possible to generate deterministic, but unpredictable sequences of uniformly distributed integers from a single input number, or seed. These seemingly random numbers are called pseudorandom numbers. Throughout this thesis the terms random and pseudorandom are used interchangably. One common algorithm for generating pseudorandom numbers is the Mersenne twister[20]. It produces integers from 0 to $2^{64} - 1$.

From the uniformly distributed integers it is possible to generate uniformly distributed floating points numbers on the interval $[0, 1]$. Let X represent the

random integers produced by the Mersenne Twister, then the random variable Y given by

$$Y = \frac{X}{2^{64} - 1},$$
(3.25)

is a random real number continuously (for all intents and purposes) distributed on the interval $[0, 1]$.
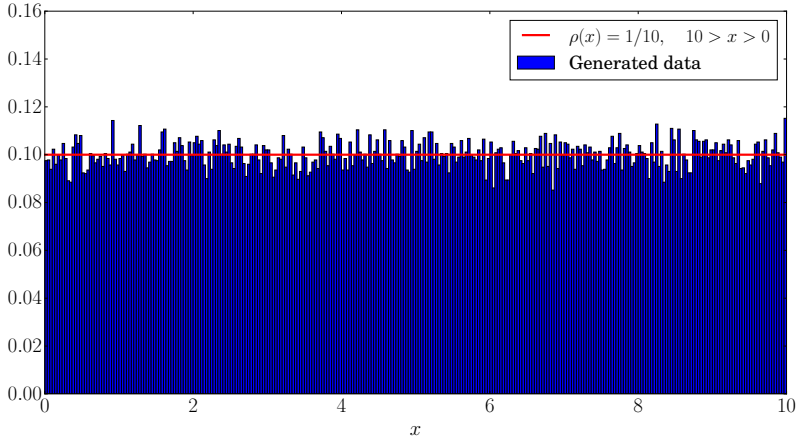

Figure 3.1. A histogram of $100,000$ uniformly distributed real numbers on the interval $[0, 10]$. The observed mean and standard deviation are $\mu^* = 5.008$ and $\sigma^* = 2.886$. The density expectation and standard deviation are $\mu = 0.5$ and $\sigma = 10/\sqrt{12} \approx 2.886$.

3.6.1   General Probability Distributions

Once a continuously and uniformly distributed random variable is achieved it is possible to generate many other continuous distributions by use of the inverse transform method[21]. For a desired random variable Y with the cumulative distribution function $F_Y(y)$ the formula is given by

$$Y = F_Y^{-1}(X),$$
(3.26)

where F_Y^{-1} is the inverse function of F_Y and X is a real random number on the interval $[0, 1]$.

In particular for this thesis exponentially distributed random numbers are required. The cumulative distribution function of the exponential function with a parameter λ is

$$F_Y(y) = 1 - e^{-\lambda y},$$
(3.27)
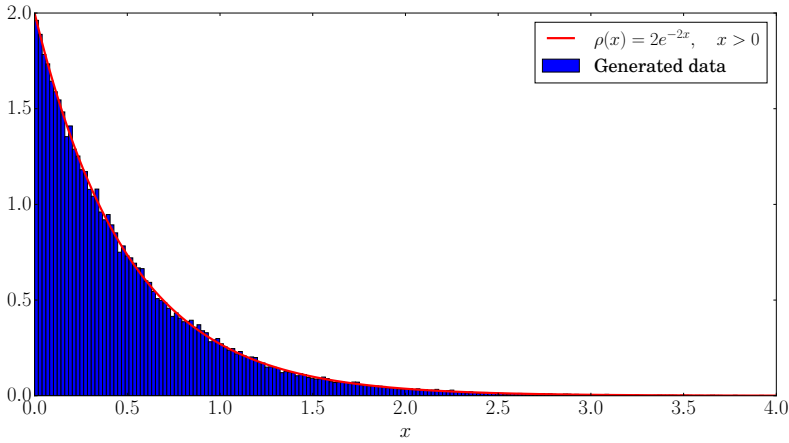
Figure 3.2. A histogram of $100,000$ exponentially distributed real numbers with parameter value $\lambda = 2$. The observed mean and standard deviation are $\mu^* = 5.007$ and $\sigma^* = 0.5013$. The density expectation and standard deviation are $\mu = 1/2$ and $\sigma = 1/2$.

so the inverse sampling formula gives

$$Y = -\frac{1}{\lambda} \ln\left(1 - X\right). \tag{3.28}$$

Once a formula for a certain distribution is implemented in code it is reasonable to test if the random numbers are distributed as desired. This can be done by generating a large set of numbers $\{x_i\}$ and generate a histogram from them. The histogram should have the same shape as the functional form of the distribution. For further validation one may also calculate the sample mean μ^* and standard deviation σ^* of the generated data and compare to the expectation μ and standard deviation σ of the corresponding probability density of function. In Fig. 3.1 and Fig. 3.2 tests of two of the implemented distributions are shown in the form of normalized histograms.

3.7 Implementation

The simulation program for this thesis implements both the Metropolis and the Wolff algorithms described in sections 3.2 and 3.3, and is written in C++. The program is capable of simulating both the classical two-dimensional Ising model and the disordered variant corresponding to the quantum Ising model (2.18).

The validity of the implementations of the two algorithms has been tested by simulating the classical ordered two-dimensional Ising model and comparing data to

analytical solutions. As a further consistency check results from the two algorithms was compared for a small size of the disordered system and were found to produce mutually consistent data. All data was produced using the Wolff algorithm during the production runs.

Another test that was performed was comparing the improved estimator with a non-improved estimator for the correlation for a smaller system. The two estimators were found to produce consistent results.

For random number generation the GCC implementation of the Mersenne twister, mt19937_64, has been used, which produces unsigned 64 bit integers uniformly on the interval from 0 to $2^{64} - 1$. The seeds have been produced by reading 64 bits from /dev/urandom, a special file available on Unix-like operating systems with the specific purpose of providing sufficiently random seeds by reading noise from various source in the computer.

Simulations have been run on a personal laptop equipped with an Intel i7-3667U CPU, and on the Octopus cluster provided by the Department of Physics at KTH, and which is equipped with Intel Xeon E5-2620 CPUs. Multiple simulations have been run in parallel, which significantly reduces the physical time to obtain the data for the thesis.

Data analysis and graphical representation was performed in Python using the packages NumPy and Matplotlib.

Chapter 4

Results

4.1 Equilibration time

At the start of each production run the system is initialized to some arbitrary state. The system is then propagated from this starting state using the Monte Carlo algorithm, and after some time the system reaches a distribution of states that obeys the Boltzmann distribution. However, there is a transient period in the beginning during which the generated states are not distributed properly. In order to avoid systematic errors no measurements are made for a number of sweeps. This is known as the equilibration of the system. The length of this transient depends on several aspects, such as system and algorithm.

Naturally the question arises as to how many sweeps should be discarded. The most practical approach to evaluating this is to observe some measurable as a function of simulation time. One way to do this is to set up two systems with the same realization of couplings K_i and fields H_i in two distinguishable initial configuration, such as the completely ordered configuration where all spins are aligned, and the completely disordered configuration, where the direction of each spin is chosen at random. These two initial configurations are distinguished by their magnetization, the ordered phase with $|m| = 1$ and the disordered phase with $|m| = 0$ on average. Then the magnetization is measured over the intervals of $0 - 1$, $1 - 2$, ..., $2^{12} - 2^{13}$ sweeps for the two initial configurations. By plotting the magnetizations for the two configurations against upper limit of the intervals it is possible to estimate the equilibration time as the time where the two initial configurations agree on the value of the average magnetization. In Fig. 4.1 the results of this scheme is shown. For the production runs of this thesis 4000 sweeps of equilibration was performed.
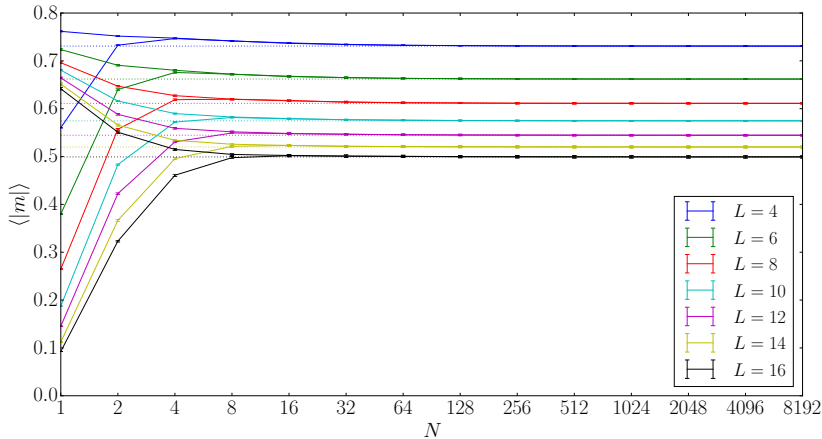
Figure 4.1. The magnetizations of the initially disordered state and the initially ordered state for the system sizes considered in this work. The x-coordinate represents the upper limit of the interval over which the corresponding magnetizations have been measured. In other words $N = 128$ represents data collected between sweep 64 and 128. The perforated lines are the final value of the initially disordered system for each corresponding L.

4.2   Main results

In this section the main results of this thesis are presented. In order to study the correlation function of the system at the critical point the critical point has to be determined first. This involves determining a specific value of the inverse temperature L_τ as well as finding the critical field T_c. This is done by studying the Binder cumulant

$$g = \frac{1}{2}\left[3 - \frac{\langle m^4 \rangle}{\langle m^2 \rangle^2}\right]_{\mathrm{av}}, \tag{4.1}$$

where the square brackets denote average over different disorder realizations of the system and angular brackets denote thermal average within one simulation.

A total of 7 system sizes have been studied starting from $L = 4$ up to $L = 16$ in increments of 2. For each disorder realization of the system a warmup of 4000 sweeps were performed, followed by a measurement phase of $40,000$ sweeps. In order to find the critical point T_c several values of L_τ have been simulated for each L. The details regarding the method for determining the critical point is discussed next section. The number of disorders which have been simulated for each value of L_τ varies between 10^4 and 10^6, with efforts focused towards the points near the maxima of g. Based on the work by Pich and Young[10, 11] the critical point was expected to be located near $T = 0.98$. Using the histogram method detailed in

Sec. 3.4 a number of 141 linearly separated values of T was extrapolated to on the interval from $T = 0.9$ up to $T = 1.04$.
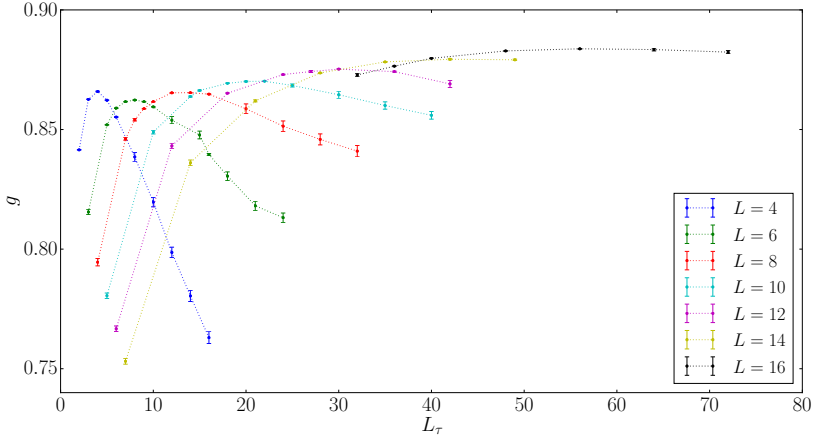

Figure 4.2. The values of g is plotted against the inverse temperature L_τ for various system sizes, with field strength $T = 0.9$. An indication of the presence of finite size scaling corrections can be seen in that the peak of the smallest size is larger than the peak of the following size. Errors are estimated using the standard error of the mean.

4.2.1 Critical Point and Corrections to Scaling

The method for localizing the critical point is described in many sources, for instance see Refs. [22, 23]. It consists in simulating the system at a number of values for the inverse temperature L_τ and fields T. As was described in Sec. 2.2.2 the Binder cumulant vanishes for the disordered phase, while it takes a finite value in the ordered phase. When the L_τ is small compared to L the system is a classical one-dimensional system. The one-dimensional classical Ising model does not exhibit a phase transition, and only exists in a disordered state for finite temperatures. For $L_\tau \gg L$ the system also becomes effectively one-dimensional and thus disordered. Between these two limits there is a region where the system is two-dimensional, and well below its critical point. Thus it is expected that that the Binder cumulant is a peaked curve as a function of L_τ, with a maximum $g = g^{\max}$ at some point $L_\tau = L_\tau^{\max}$, which depends on L.

The value of $g^{\max}$ depends on the value of T. For $T < T_c$ the maximum $g^{\max}$ increases as L increases, while for $T > T_c$ it decreases with increasing L, as can be seen in Figs. 4.2 and 4.3. At the critical point $T = T_c$ the maximum is expected to
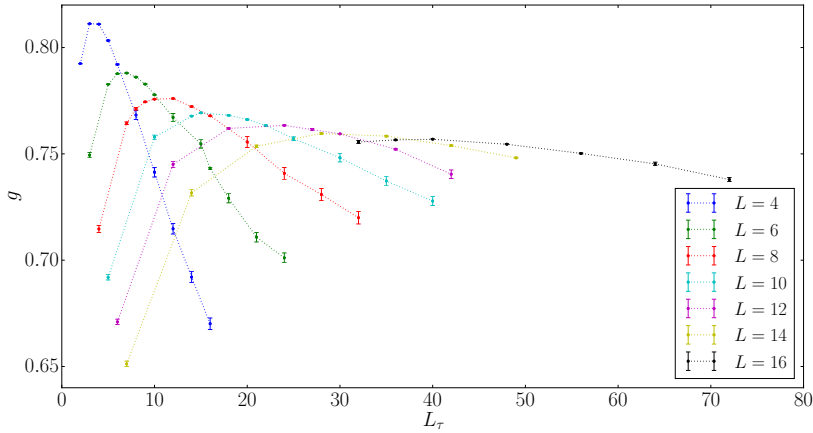
Figure 4.3. The values of g is plotted against the inverse temperature L_τ for various system sizes, with field strength $T = 1.04$. Errors are estimated using the standard error of the mean.

be independent of L. Additionally, from the work of Fisher[8, 9] it is expected that $L_\tau^{\max}$ scales according to

$$\ln L_\tau^{\max} \sim L^z \tag{4.2}$$

with $z = 1/2$. This type of scaling behavior is known as activated dynamic scaling.

The expectation that $g^{\max}$ at the critical point is independent of the system size L does not take into account the effects of finite size scaling corrections. Including such effects $g^{\max}$ is instead expected to scale with L as

$$g^{\max} = g_0 + g_1 L^{-\omega}, \tag{4.3}$$

where g_1 and ω are correction parameters, and g_0 a constant. In Fig. 4.2 a clear indication of the existence of corrections in the form of (4.3) can be seen. In order to determine the critical point the four parameters T_c, g_0, g_1 and ω need to be determined simultaneously.

The first step in order to optimize these four parameters is to determine the value of $g^{\max}$ closely for each size L. In Fig. 4.4 it can be seen that the curves of g behave smoothly when plotted against $\ln L_\tau$, indicating that it is possible to obtain estimates of $g^{\max}$ by fitting the data to a second order polynomial in powers of $\ln L_\tau$. This gives a functional form of g around the maximum as

$$g_{\text{fit}}\left(L_\tau\right) = c_2 \left(\ln L_\tau\right)^2 + c_1 \ln L_\tau + c_0. \tag{4.4}$$
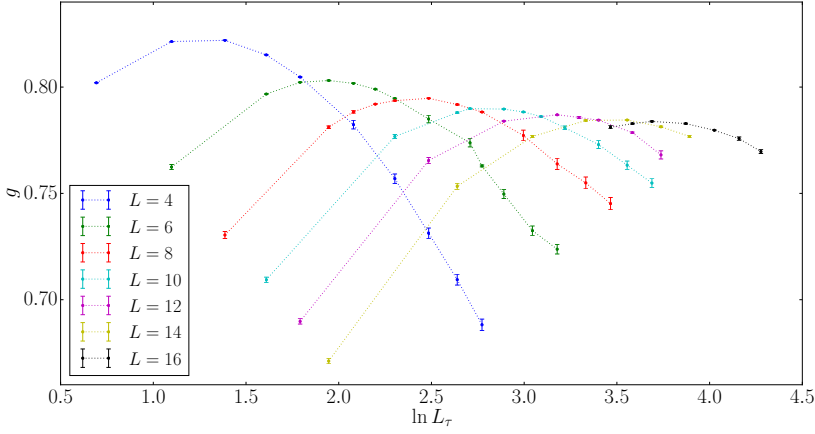
Figure 4.4. The values of g is plotted against $\ln L_\tau$ for various system sizes, with field strength $T = 1.013$. Errors are estimated using the standard error of the mean.

From this fit $L_\tau^{\max}$ and $g^{\max}$ are given by

$$g^{\max} = -\frac{c_1^2}{4c_2} + c_0, \tag{4.5}$$

$$L_\tau^{\max} = e^{-\frac{c_1}{2c_2}}. \tag{4.6}$$

For each fit five points were used and the points chosen were the point with the maximum numerical value and the 4 points closest to it.

Next it is noted that Eq. (4.3) can be rewritten as

$$\ln\left(g^{\max} - g_0\right) = -\omega \ln L + \ln g_1. \tag{4.7}$$

Given a value of g_0 the left hand side can be fitted to $\ln L$ in order to determine optimal values for g_1 and ω.

To determine an optimal value for g_0 the straightforward approach has been taken of setting up an interval of linearly separated values for g_0 for which g_1 and ω has been computed. Given these three parameter values the fit of $g^{\max}$ was assessed by computing

$$\chi^2 = \sum_{i=1}^{N} \frac{\left(g_{L_i}^{\max} - g^{\max}\left(L_i\right)\right)^2}{\sigma_i^2}, \tag{4.8}$$

where $g_{L_i}^{\max}$ are the observed maxima, $g^{\max}(L)$ is the fit given by (4.3), and σ_i are the estimated errors of the maxima $g_{L_i}^{\max}$. The value of g_0 which gives the lowest value of χ^2 was stored for each value of T. In Fig. 4.5 the values of χ^2 for the stored g_0 of each T are shown. The curve has a minimum at approximately $T = 1.013$.
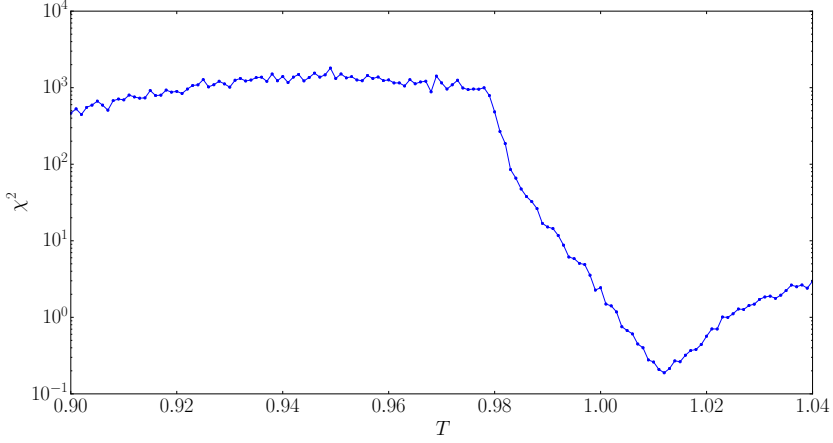
Figure 4.5. The values of χ^2 for the best value of g_0 plotted against corresponding field T. A clear minimum can be identified for values around $T = 1.013$.
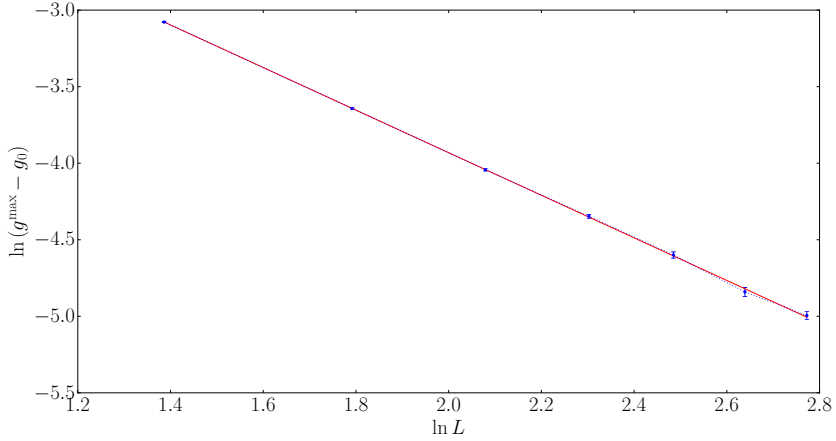

Figure 4.6. The logarithm of the difference $g^{\max} - g_0$ plotted against $\ln L$, at field $T = 1.013$. The error bars have been calculated from the bootstrap errors of $g^{\max}$ using the propagation of error formula.
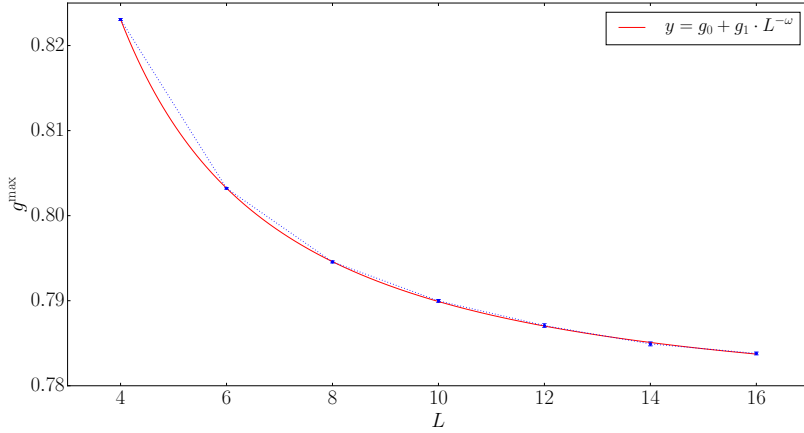
Figure 4.7. The interpolated maximum values of g plotted over the corresponding system sizes L at the critical field $T = T_c$. The fit given by determining the parameters for the correction to scaling is also shown and supports the suggested correction form of (4.3). The error bars are produced using bootstrap estimation.

param	value
T_c	1.013
g_0	0.777
g_1	0.3166
ω	1.3907

Table 4.1. Best values obtained from the finite size scaling correction analysis. No formal estimation of errors has been performed.

This value is taken as the critical point $T_c = 1.013$. The corresponding values of g_0, g_1 and ω constitute the best estimates for the finite size scaling corrections, and the numerical values are displayed in along with T_c in Tab. 4.1.

In Fig. 4.6 the values of $\ln(g^{\mathrm{max}} - g_0)$ are shown against $\ln L$ for $T = T_c$ and corresponding g_0 along with the linear fit to the data, while in Fig. 4.7 the values of g^{max} against L are shown together with the fit given by (4.3) using the values of Tab. 4.1. From these figures it can be concluded that the hypothesis of the scaling corrections of the form (4.3) is well supported by the data.
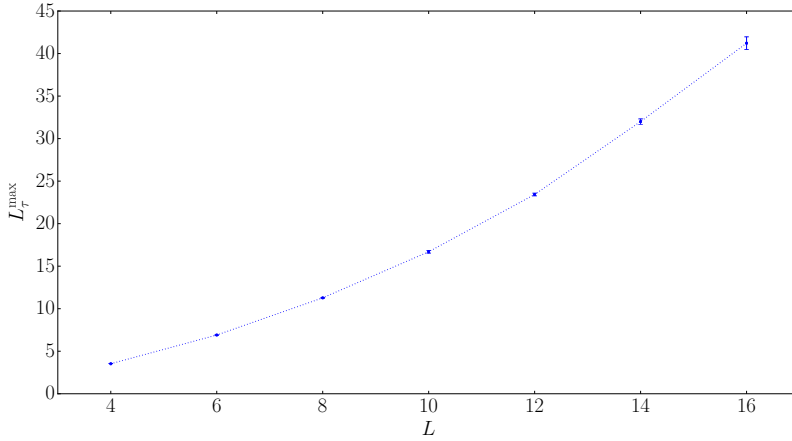
Figure 4.8. The interpolated maximum values of L_τ plotted over the corresponding system sizes L. The curvature of the data indicates that the scaling of the disordered system deviates from the ordered system, for which the same plot would yield a straight line. The error bars are produced using bootstrap estimation.

4.3   Comparison with Analytical Results

Once the location of the critical point has been located the numerical results can be compared with the analytic predictions discussed in Sec. 2.6. For the ordered quantum Ising model the $L_\tau^{\max}$ is known to scale as L^z with $z = 1$ at the critical point $J = h$. For the disordered system it is predicted that the location of the $L_\tau^{\max}$ should scale as

$$\ln L_\tau^{\max} \sim L^z, \tag{4.9}$$

and if the Binder cumulant is plotted against $\ln L_\tau^{\max}/L^z$ with $z = 1/2$ the data should collapse to the universal scaling function. In Figs. 4.8 - 4.10 various scaling tests are shown for L_τ.
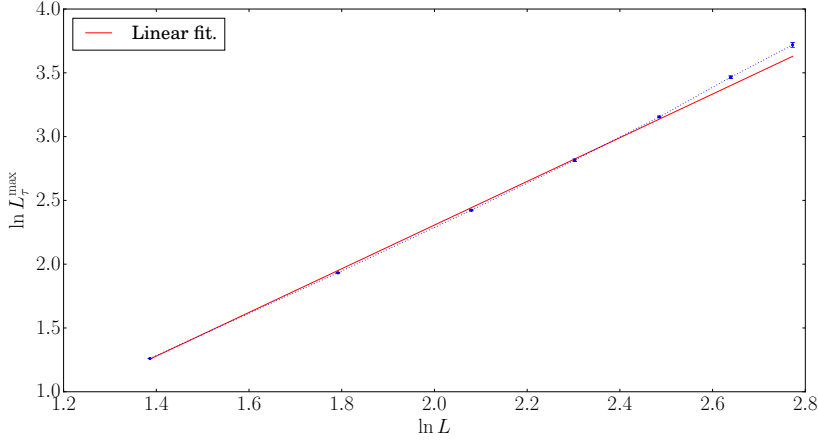
Figure 4.9. The logarithm of the interpolated maximum values of L_τ plotted over the logarithm of corresponding system sizes L. The deviation from the linear fit of the larger sizes seem to indicate that the the scaling of $L_\tau^{\max}$ is not of the form $L_\tau^{\max} \sim L^z$. The error bars are calculated using the propagation of error formula.
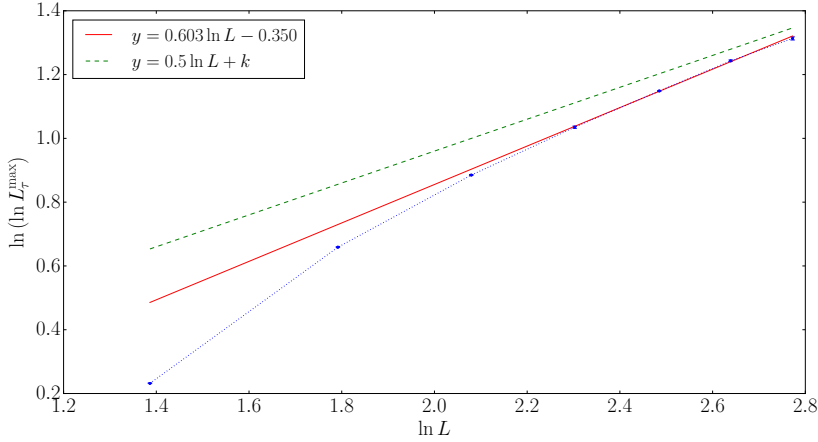

Figure 4.10. The values of $\ln \left(\ln L_\tau^{\max}\right)$ plotted against $\ln L$. The red line represents a linear fit to the rightmost four data points, which closest resembles a line. The green line is added for reference to show the slope expected due to analytic predictions. The deviation of the fit from the analytic slope may be explained by the existence of scaling corrections. The error bars are calculated using the propagation of error formula.
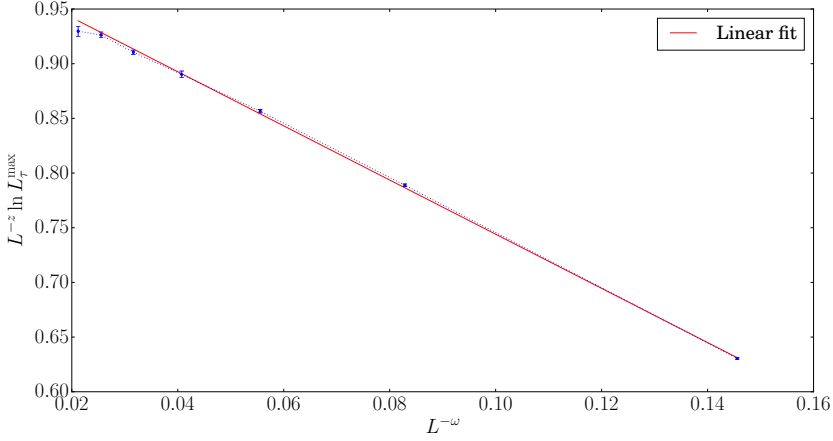
Figure 4.11. The rescaled quantity $L^{-z} \ln L_\tau^{\max}$ is plotted against $L^{-\omega}$, where $z = 1/2$ and $\omega = 1.3907$. The data is consistent with the corrected scaling form of Eq. (4.10). The error bars are calculated using the propagation of error formula.

In particular it is expected in Fig. 4.10 to see a linear dependence of $\ln \left(\ln L_\tau^{\max} \right)$. This does not occur, but the curvature seems to decrease for larger L, and it seems plausible that the correct scaling may be observed for even larger systems. This suggests that also $L_\tau^{\max}$ exhibits scaling corrections. To lowest order the corrected scaling form for $\ln L_\tau$ is expected to be in the form

$$\ln L_\tau^{\max} \sim L^z \left(1 + k L^{-\omega} \right), \tag{4.10}$$

where k is a constant, $z = 1/2$ is the uncorrected scaling exponent, and ω is the correction exponent determined in previous section. From (4.10) it stands clear that plotting $L^{-z} \ln L_\tau^{\max}$ against $L^{-\omega}$ should produce a linear graph. This behavior is quite convincingly confirmed in Fig. 4.11.

In Fig. 4.12 the values of g have been modified by subtraction of the scaling corrections, and are plotted against the logarithm of $L_\tau / L_\tau^{\max}$. There seems to be a tendency for the curves to broaden away from $L_\tau^{\max}$, which is expected according to the activated dynamic scaling, however due to the large error bars predictions are unreliable. In Fig. 4.13 the same corrected values of g from Fig. 4.12 are plotted against $\ln L_\tau / \ln L_\tau^{\max}$, which is expected to be the correct scaling. Smaller sizes significantly deviate from this scaling and have been omitted. For the larger sizes the scaling is not disproved, but there are too few data points away from the maximum and too large error bars to make a claim either way.
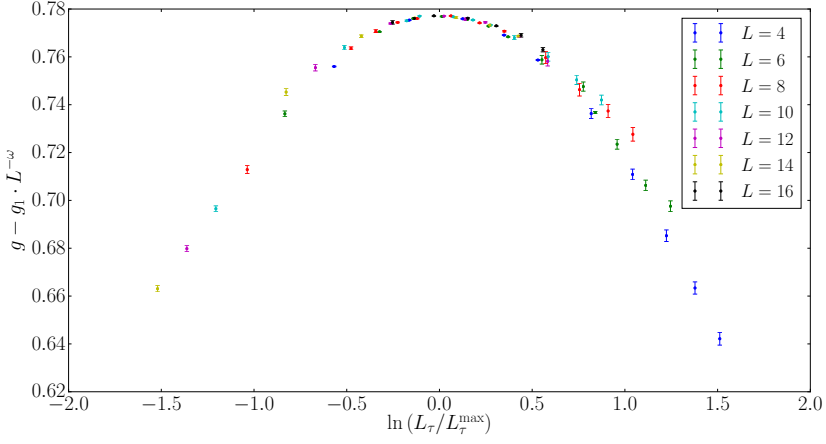
Figure 4.12. The values of $g - g_1 \cdot L^{-\omega}$ is plotted against $\ln \left(L_\tau / L_\tau^{\max} \right)$.
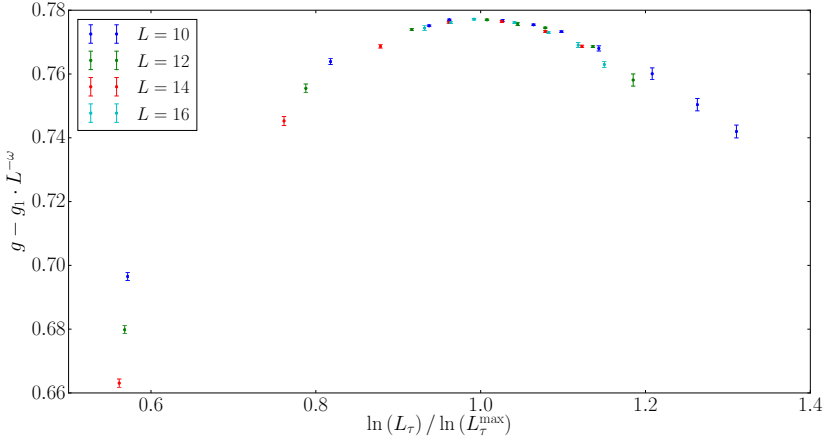

Figure 4.13. The values of $g - g_1 \cdot L^{-\omega}$ is plotted against $\ln L_\tau / \ln L_\tau^{\max}$. The three smallest sizes have been excluded as they do not scale very well, suggesting the presence of higher order corrections to scaling.
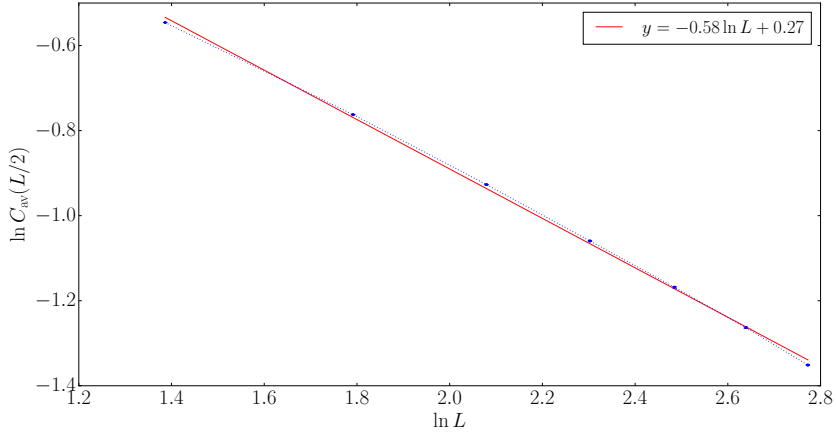
Figure 4.14. Values of $\ln C_{\mathrm{av}}\left(L/2\right)$ against $\ln L$. The slope of the linear fit is inconsistent with the corresponding analytic value.
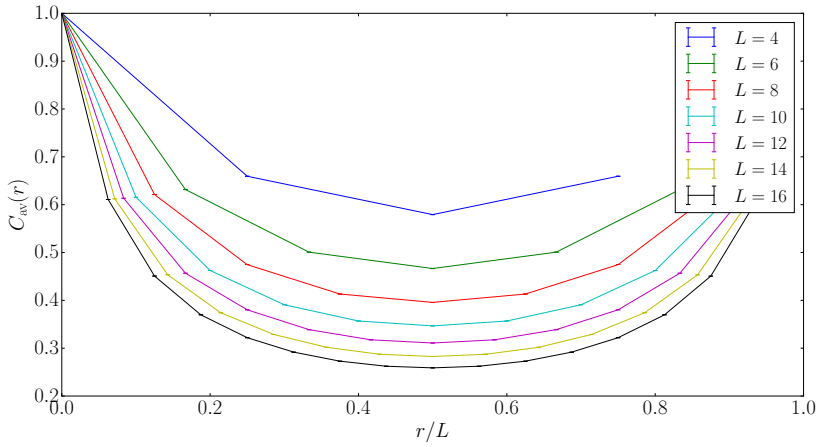

Figure 4.15. The average correlation $C_{\mathrm{av}}\left(r\right)$ for each system size at the critical field $T = 1.013$.

Another result due to Fisher is the scaling of the typical correlation C_{typ} and that of the average correlation C_{av}. The average correlation $C_{\mathrm{av}}\left(r\right)$ at the critical point T_c is expected to scale as

$$C_{\mathrm{av}}\left(r\right) \sim r^{-\lambda}. \tag{4.11}$$

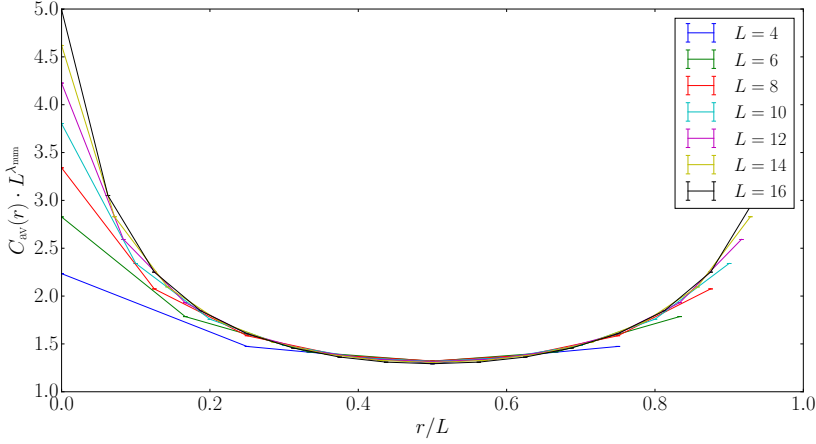**Figure 4.16.** The average correlation $C_{av}(r)$ rescaled by a size dependent factor $L^{\lambda_{num}}$, with $\lambda_{num} = 0.58$.

Analytically the exponent was found to be $\lambda = 2 - \varphi$, where φ is the golden ratio $\varphi = \frac{1-\sqrt{5}}{2}$, which gives a value of $\lambda \approx 0.38$. From (4.11) follows that

$$L^{-\lambda}C_{av}(r) \sim x^{-\lambda}, \tag{4.12}$$

where $x = r/L$. Thereby the shape of $L^{-\lambda}C_{av}(r)$ should be independent of the system size. Another observation that can be made is that

$$\ln C_{av}(L/2) = -\lambda \ln L + \text{const.} \tag{4.13}$$

Thereby it should be possible to obtain the critical exponent by plotting $\ln C_{av}(L/2)$ against $\ln L$ and fitting the data to a straight line. This is done in Fig. 4.14, however the data suggests an exponent of $\lambda_{num} = 0.58$, which substantially deviates from the prediction. This deviation could not be compensated for by corrections to scaling as it could for L_τ^{max}. In Fig. 4.15 the average correlation is plotted against x, while in Fig. 4.16 the rescaled correlation $L^\lambda C_{av}$ is shown against x. The rescaled correlation does not collapse very well away from $L/2$ when using λ_{num} obtained from the slope of the linear fit of Fig. 4.14. For comparison the numerical value for λ as was obtained by Pich and Young was $\lambda_{PY} = 0.5$, a value comparable to the value obtained here. As to why the numerical values differ from the analytic no answer has been found during the work of this thesis.
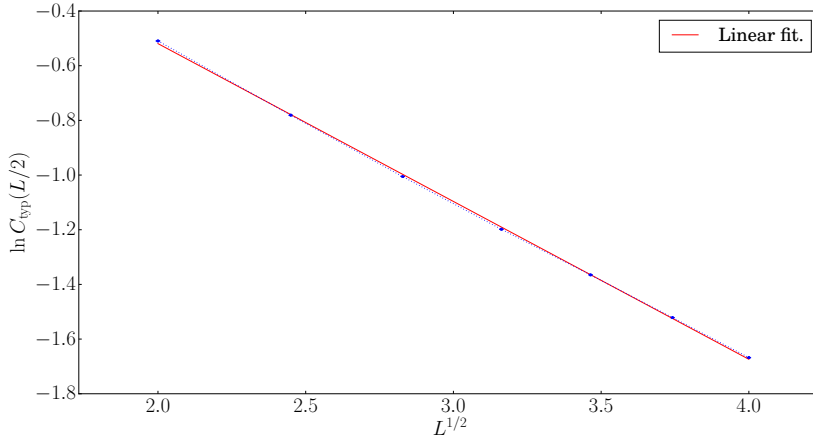
Figure 4.17. Values of the typical correlation $C_{\mathrm{typ}}(L/2)$ plotted against $L^{1/2}$. There are small deviations from the linear fit, which are expected to be due to scaling corrections.

For the typical correlation $C_{\mathrm{typ}}(r)$ it is expected that

$$\ln C_{\mathrm{typ}}(r) \sim r^{-1/2}. \tag{4.14}$$

Plotting $\ln C_{\mathrm{typ}}(r)$ against $L^{-1/2}$ should therefore produce a linear graph. Following the example set by Pich and Young the typical value has been estimated by the median. In Fig. 4.17 the values of $C_{\mathrm{typ}}(L/2)$ are plotted against $\ln L$, and the data seem to fit well to the linear relation. The small deviations from the linear relation is most likely attributable to scaling corrections.

In Figs. 4.18 and 4.19 histograms of the correlation function is provided to illustrate qualitatively the shape of the distribution of $C(r)$. Notably the distributions are very wide, which is what induces the difference in behaviour between the average and typical correlations.
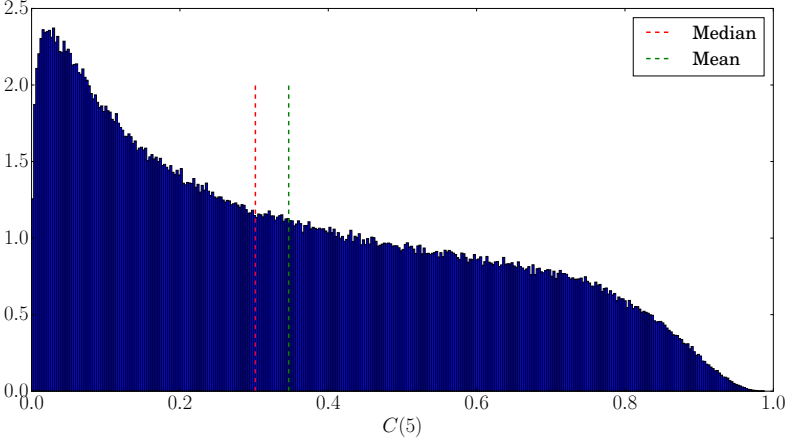
Figure 4.18. Histogram of the correlation function $C(5)$ for system size $L = 10$.
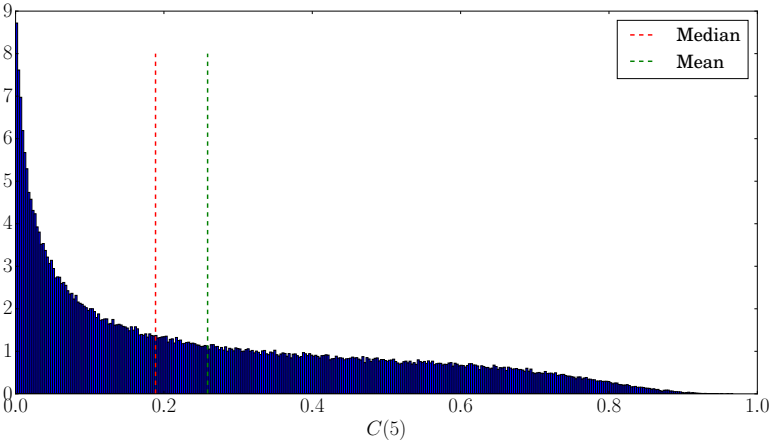

Figure 4.19. Histogram of the correlation function $C(8)$ for system size $L = 16$.

Chapter 5

Summary, Discussion and Outlook

5.1 Summary

In this thesis the quantum phase transition of the one-dimensional transverse field random Ising model has been studied numerically by mapping the system to the corresponding two-dimensional classical Ising model. To this end an implementation of the Wolff algorithm in C++ written specifically for this thesis has been used.

The data obtained has smaller error bars than previous work by Pich and Young[10, 11], partly due to the availablility of more powerful computers today, but also due to the simulations being restricted to smaller system sizes. Additionally by including even smaller systems than the previous work the effects of finite size scaling corrections can be observed and analyzed. When the finite size scaling corrections are accounted for a modified value of the critical point for the parametrizing variable for the field $T_c = 1.013$ is found, as compared to previous value of $T_c = 0.98$.

Analytical predictions due to Fisher[8, 9] are tested. The scaling of the Binder cumulant g is investigated and it seems that the data does not collapse well when plotted against $L_\tau / L_\tau^{\max}$, but rather seems to widen as L is increased, which should indicate activated dynamic scaling. It is further shown that the scaling behavior of $\ln L_\tau^{\max}$ is consistent with activated dynamic scaling, provided that corrections to scaling are accounted for.

Additionally, analytic predictions regarding the correlation function have been tested. The average correlation C_{av} is expected to scale as $C_{\mathrm{av}} \sim r^{-\lambda}$ with $\lambda \approx 0.38$. This is not reproduced in the numerics, where instead the best estimate is found to be $\lambda_{\mathrm{num}} = 0.58$, which is comparable to previous result of $\lambda_{\mathrm{PY}} = 0.5$ obtained by Pich and Young. This value of λ_{num} does not collapse the average correlation

very well. Simultaneously the typical correlation C_{typ} is expected to show the scaling behaviour $C_{\text{typ}} \sim e^{-kr^{1/2}}$. Following the example of Pich and Young the typical correlation has been estimated using the median over the set of realizations of disorders. By plotting $\ln C_{\text{typ}}(L/2)$ against $L^{1/2}$ it is shown that the typical correlation scales just as predicted by analytical work.

Overall all data obtained in this thesis has been found to be largely consistent with the data from Pich and Young. The main new result is the measurement of the exponent $\omega = 1.39$ of the correction to scaling, which enables performing a more accurate finite size scaling analysis than was obtained by Pich and Young. The discrepancy between the numerical and analytical value of the critical exponent of C_{av} remains unresolved.

5.2   Outlook

In this thesis the focus was put on smaller system sizes in order to obtain accurate data with small statistical error. The most direct extension to this thesis would be to go beyond the smaller system sizes in order to obtain better estimates for the exponent ω of the correction to scaling. Additionally, it may be of interest to explore larger and smaller values of L_τ more extensively than was done here. This may allow the activated dynamic scaling to be seen more clearly when rescaling the Binder cumulant.

Another point of interest would be to study if a system subject to frustration would also display the peculiar behaviour of differing typical and average behaviour of thermodynamic quantities as the nonfrustrated system. It is not possible to introduce frustration directly to the one-dimensional chain system studied here, so the geometry must be modified in some way. An issue that arises when dealing with frustrated systems is that the Binder cumulant can no longer be used. A different parameter is required in order to locate the critical point of the system. During the work of this thesis one quantity that may work was tried out briefly, defined by $\delta E \equiv (\langle E_{\text{pbc}} \rangle - \langle E_{\text{apbc}} \rangle)^2$, where E_{pbc} denotes the energy of the system with periodic boundary condition and E_{apbc} the same disorder realization, but with antiperiodic boundary condition. This requires each system to be simulated twice, increasing the computational cost by a factor 2. Pursuing this direction remains a challenge for future work.

Bibliography

[1] R. B. Griffiths, *Dependence of Critical Indices on a Parameter*, Physical Review Letters **24**, 1479 (1970).

[2] L. P. Kadanoff, *Scaling laws for ising models near T_c*, Physics Physique Fizika **2**, 263 (1966).

[3] K. G. Wilson, *Renormalization Group and Critical Phenomena. I. Renormalization Group and the Kadanoff Scaling Picture*, Physical Review B **4**, 3174 (1971).

[4] M. Suzuki, *Relationship between d-Dimensional Quantal Spin Systems and (d+1)-Dimensional Ising Systems: Equivalence, Critical Exponents and Systematic Approximants of the Partition Function and Spin Correlations*, Progress of Theoretical Physics **56**, 1454 (1976).

[5] S. Sachdev, *Quantum Phase Transitions*, 2 ed. (Cambridge University Press, 2011).

[6] D. Bitko, T. F. Rosenbaum and G. Aeppli, *Quantum Critical Behavior for a Model Magnet*, Physical Review Letters **77**, 940 (1996).

[7] R. Coldea *et al.*, *Quantum Criticality in an Ising Chain: Experimental Evidence for Emergent E8 Symmetry*, Science **327**, 177 (2010).

[8] D. S. Fisher, *Random transverse field Ising spin chains*, Physical Review Letters **69**, 534 (1992).

[9] D. S. Fisher, *Critical behavior of random transverse-field Ising spin chains*, Physical Review B **51**, 6411 (1995).

[10] C. Pich and A. P. Young, *Critical Behavior of the Two-Dimensional Random Quantum Ising Ferromagnet*, arXiv e-prints , cond (1998), `cond-mat/9802108`.

[11] C. Pich *et al.*, *Critical Behavior and Griffiths-McCoy Singularities in the Two-Dimensional Random Quantum Ising Ferromagnet*, Physical Review Letters **81** (1998).

[12] M. Plischke and B. Bergersen, *Equilibrium Statistical Physics*, 3rd ed. (World Scientific, 2006).

[13] N. Goldenfeld, *Lectures On Phase Transitions And The Renormalization Group* (CRC Press, 2018).

[14] K. Binder, *Critical Properties from Monte Carlo Coarse Graining and Renormalization*, Physical Review Letters **47**, 693 (1981).

[15] H. F. Trotter, *On the Product of Semi-Groups of Operators*, Proceedings of the American Mathematical Society **10**, 545 (1959).

[16] M. Newman and G. Barkema, *Monte Carlo Methods in Statistical Physics* (Clarendon Press, 1999).

[17] W. K. Hastings, *Monte Carlo Sampling Methods Using Markov Chains and Their Applications*, Biometrika **57**, 97 (1970).

[18] U. Wolff, *Collective Monte Carlo Updating for Spin Systems*, Physical Review Letters **62**, 361 (1989).

[19] B. Efron, *Bootstrap Methods: Another Look at the Jackknife*, The Annals of Statistics **7**, 1 (1979).

[20] M. Matsumoto and T. Nishimura, *Mersenne twister: a 623-dimensionally equidistributed uniform pseudo-random number generator*, ACM Transactions on Modeling and Computer Simulation **8**, 3 (1998).

[21] L. Devroye, *Non-Uniform Random Variate Generation* (Springer New York, 1986).

[22] M. Guo, R. N. Bhatt and D. A. Huse, *Quantum critical behavior of a three-dimensional Ising spin glass in a transverse magnetic field*, Physical Review Letters **72**, 4137 (1994).

[23] H. Rieger and A. P. Young, *Zero-temperature quantum phase transition of a two-dimensional Ising spin glass*, Physical Review Letters **72**, 4141 (1994).